

Variational Knowledge Distillation for Disease Classification in Chest X-Rays

Tom van Sonsbeek¹, Xiantong Zhen^{1,2}, Marcel Worring¹, and Ling Shao²

¹ University of Amsterdam, The Netherlands

² Inception Institute of Artificial Intelligence, U.A.E

{t.j.vansonsbeek, x.zhen, m.worring}@uva.nl, ling.shao@ieee.org

Abstract. Disease classification relying solely on imaging data attracts great interest in medical image analysis. Current models could be further improved, however, by also employing Electronic Health Records (EHRs), which contain rich information on patients and findings from clinicians. It is challenging to incorporate this information into disease classification due to the high reliance on clinician input in EHRs, limiting the possibility for automated diagnosis. In this paper, we propose *variational knowledge distillation* (VKD), which is a new probabilistic inference framework for disease classification based on X-rays that leverages knowledge from EHRs. Specifically, we introduce a conditional latent variable model, where we infer the latent representation of the X-ray image with the variational posterior conditioning on the associated EHR text. By doing so, the model acquires the ability to extract the visual features relevant to the disease during learning and can therefore perform more accurate classification for unseen patients at inference based solely on their X-ray scans. We demonstrate the effectiveness of our method on three public benchmark datasets with paired X-ray images and EHRs. The results show that the proposed variational knowledge distillation can consistently improve the performance of medical image classification and significantly surpasses current methods.

Keywords: Multi-modal learning · Medical Image Classification · Electronic Health Records · Knowledge Distillation · Variational Inference.

1 Introduction

Advances in deep learning for medical imaging have been shown to perform on par or better than clinicians on an increasing number of tasks [17]. The expansion of data and computational resources has played a large role in this. In fact, while deep learning models and clinicians may seem very different at first, their underlying prediction process is similar, as they both acquire experience through data. However, clinicians currently have an advantage; their decision making is not only based on medical images. In addition to their own knowledge and experience, information on the patient can also provide important guidance when making a diagnosis. Thus, there is an opportunity for deep learning methods to be even further improved if they could also incorporate this information.

EHRs contain rich information about the patients, which could be explored for disease classification based on X-ray scans. Besides important patient information, e.g., disease history, sex and reason for hospital admission, they record observations and findings that are usually provided by clinicians from reading the scans in combination with their professional knowledge and clinical experiences. It has been demonstrated that (longitudinal) EHR data can be used as a diagnosis predictor [2, 7, 28, 35]. Thus it would be greatly helpful to if we can leverage EHRs to support clinicians by improving the performance of various automated medical imaging tasks.

However, it is a challenging problem to incorporate information from EHRs into medical image analysis due to several reasons. Firstly, representing EHR in models is complicated by the large variety in content, structure, language, noise, random errors, and sparseness [2, 28]. Secondly, there are privacy concerns in using medical images associated with (longitudinal) EHR data, as their combined use limits the extent of possible anonymization [33]. However the major limiting factor is that combining visual and textual modalities adds complexity, because it requires methods that span both vision and language processing fields.

From a clinical point of view, the usage of EHR data available during testing or model deployment should be approached with caution, because EHR data is not always available coupled to the patient at the time of diagnosis. It is important to keep in mind that tasks performed on medical data are only relevant in a clinical setting. Requiring EHR data as input for a model would prevent this model from being completely automated, because the EHR still needs to be created by a clinician. However, this is not a problem during training when access to large databases of medical images and EHRs is possible. Therefore, to effectively utilize EHRs in combination with medical images, they should be optimally utilized during training time, with minimum reliance on them during testing. In a clinical setting, this would make most sense, because we would like the model to assist clinicians rather than relying on them.

It is particularly appealing to leverage information in EHRs for disease classification of X-ray scans. This is because chest X-rays are one of the most common scans in clinical routines due to their ease of acquiring and low cost, offering an effective and efficient tool for screening various diseases. A consequence of this is a large quantity of scans, the bulk of which will fall under a frequent set of diagnoses. Both the potential usefulness of EHRs and importance of automated diagnosis in clinical setting make X-rays an excellent application domain.

In this work, we tackle the challenging scenario where the EHRs are only available in the learning stage but not at inference time. We propose variational knowledge distillation, a new probabilistic inference framework to leverage knowledge in EHRs for medical image classification. We make three-fold contributions: *i*) We propose the first probabilistic inference framework for joint learning from EHRs and medical images, which enables us to explore multi-modal data during training and perform disease classification relying only on images during testing. *ii*) We introduce variational knowledge distillation, which enables the model to extract visual features relevant to disease by transferring

useful information from EHRs to images. *iii)* We demonstrate the effectiveness of the proposed method in X-ray disease classification and achieve consistently better performance than counterpart methods.

2 Related Work

In recent years there has been an increase in methods exploring automated diagnosis from radiology images. This can be linked to the increasing availability of public chest X-ray datasets, such as ChestX-ray14 [31], CheXpert [11], OpenI [20] and MIMIC-CXR [12], where the latter two also contain associated EHR.

The most notable image-based approach for chest X-ray classification is ChexNet [22]. Rajpurkar *et al.* showed that diagnosis using a deep architecture based on Densenet-121 [9] can exceed radiologist performance. Wang *et al.* [31] also reached high performance using pre-trained convolutional neural network (CNN). Recently, Chen *et al.* [3] introduced a graph based model which exceeds the performance of the prior methods in this classification task.

Current multi-modal approaches for chest X-ray classification rely on EHR inputs during both training and testing. A common denominator in these methods is that image and EHR features are joined through an attention mechanism. Nunes *et al.* [19] proposed a method which requires a chest X-ray and its associated EHR to generate a diagnosis. Wang *et al.* [32] require a similar input but use an auxiliary EHR generation task in an end-to-end CNN-recurrent neural network (RNN) architecture to improve classification. Related to this, Xue *et al.* [36] generate EHRs to enhanced image-based classification. No EHR input is required or used during both training and testing. Where our approach uses both image and EHR during training, but only images during testing, their approach only requires images in both training and testing.

Recent advances in the general non-medical vision-language field have been accelerated by the emergence of contextual Transformer [29] based language models such as BERT [5]. Moreover in visual-question-answering (VQA), models such as LXMERT [27], VL-BERT [26], VILBERT [18] and Uniter [4] vastly outperform traditional state-of-the-art models. The Transformer architecture has proven to be highly effective in multi-modal settings. Recently, Li *et al.* [16] showed how these vision-language models can be applied to the medical domain. Specifically, they showed that Transformer-based vision-language models result in high performance on medical datasets containing chest X-ray images and paired EHRs, requiring both modalities as input during training and testing.

3 Methodology

We formulate the disease classification from medical images as a conditional variational inference problem. We introduce a conditional latent variable model that infers the latent representations of X-Ray images. The knowledge is transferred from the EHR to X-rays scans by making the variational posterior conditioned on the associated EHR text. The model learns the ability to extract visual features

that are relevant to the disease guided by the associated EHR in the learning stage. At inference time it is able to make accurate predictions relying solely on X-ray scans. We start with preliminaries on variational auto-encoders [15, 23], based on which we derive our probabilistic modeling of disease classification on X-rays and variational knowledge distillation from EHRs.

3.1 Preliminaries

The variational auto-encoder (VAE) [15, 23] is a powerful generative model that combines graphical models and deep learning. Given an input \mathbf{x} from a data distribution $p(\mathbf{x})$, we aim to find its representation \mathbf{z} in a latent space, from which we can generate new images that are similar to \mathbf{x} . The objective of the VAE is to maximize what is called the evidence lower bound (ELBO), as follows:

$$\mathcal{L}_{\text{VAE}} = \mathbb{E}[\log p(\mathbf{x}|\mathbf{z})] - D_{\text{KL}}[q(\mathbf{z}|\mathbf{x})||p(\mathbf{z})], \quad (1)$$

where $q(\mathbf{z}|\mathbf{x})$ is the variational posterior for approximating the exact posterior $p(\mathbf{z}|\mathbf{x})$ and $p(\mathbf{z})$ is the prior distribution over \mathbf{z} , which is usually set to an isotropic Gaussian distribution $\mathcal{N}(0, I)$. The VAE offers an effective probabilistic inference framework to learn latent representations in a unsupervised way, which we explore for the supervised, disease classification task by introducing conditioning into the probabilistic framework.

3.2 Disease Classification by Conditional Variational Inference

Since disease classification based on X-rays is a supervised learning problem, we resort to conditional variational inference, which has shown great effectiveness in structure prediction tasks [25]. Given an input X-ray image \mathbf{x}_I associated with its class label \mathbf{y} , we introduce the latent variable \mathbf{z}_I as the representation of \mathbf{x}_I . From a probabilistic perspective, predicting of the class label \mathbf{y} amounts to maximizing the following conditional log-likelihood:

$$\log p(\mathbf{y}|\mathbf{x}_I) = \log \int p(\mathbf{y}|\mathbf{x}_I, \mathbf{z}_I) p(\mathbf{z}_I|\mathbf{x}_I) d\mathbf{z}_I, \quad (2)$$

where $p(\mathbf{z}_I|\mathbf{x}_I)$ is the conditional prior over the latent representation \mathbf{z}_I (See Fig. 1). To find the posterior $p(\mathbf{z}_I|\mathbf{x}_I, \mathbf{y})$ over \mathbf{z}_I , we usually resort to a variational distribution $q(\mathbf{z}_I)$ by minimizing the Kullback-Leibler (KL) divergence

$$D_{\text{KL}}[q(\mathbf{z}_I)||p(\mathbf{z}_I|\mathbf{x}_I, \mathbf{y})]. \quad (3)$$

By applying Bayes' rule, we obtain

$$\mathcal{L}_{\text{CVI}} = \mathbb{E}[\log p(\mathbf{y}|\mathbf{x}_I, \mathbf{z}_I)] - D_{\text{KL}}[q(\mathbf{z}_I)||p(\mathbf{z}_I|\mathbf{x}_I, \mathbf{y})], \quad (4)$$

which is the ELBO of the conditionally predictive log-likelihood in Eq. (2) and can be directly maximized to learn the model parameters. Note that maximizing the ELBO is equivalent to minimizing the KL divergence in Eq. (3). Actually, we are free to design the variational posterior $q(\mathbf{z})$. In this work, we incorporate the information from EHRs into the inference of latent representation by making the variational posterior dependent on the associated EHRs during learning.

3.3 Knowledge Distillation from EHRs

We introduce a new variational posterior that depends on the corresponding EHR text \mathbf{x}_T , which enables us to distill knowledge from EHRs to the representations of images in the latent space. To be more specific, we design the variational posterior as $q(\mathbf{z}_T|\mathbf{x}_T)$, shown in Fig. 1, which gives rise to a new ELBO, as follows:

$$\mathcal{L}_{\text{VKD}} = \mathbb{E}[\log p(\mathbf{y}|\mathbf{x}_I, \mathbf{z}_I)] - D_{\text{KL}}[q(\mathbf{z}_T|\mathbf{x}_T)||p(\mathbf{z}_I|\mathbf{x}_I)]. \quad (5)$$

By maximizing the above ELBO, the distributional distance in terms of KL divergence between the latent representations of the X-ray image and its associated EHR text is minimized. This encourages the rich knowledge contained in the EHR to be transferred to the image representations.

In order to extract from the EHR the most relevant information for accurate disease classification, the latent representation \mathbf{z}_T should also be maximally predictive of the disease. This can be achieved by maximizing the mutual information $I(Z_T, Y)$ between Z_T and Y , which is intractable. Instead, we can maximize its variational lower bound inspired by [1], as follows:

$$I(Z_T, Y) \geq \int p(\mathbf{x}_T)p(\mathbf{y}|\mathbf{x}_T)p(\mathbf{z}_T|\mathbf{x}_T) \log q(\mathbf{y}|\mathbf{z}_T) d\mathbf{x}_T d\mathbf{y} d\mathbf{z}_T = \mathcal{L}_{\text{MI}}, \quad (6)$$

where $q(\mathbf{y}|\mathbf{z}_T)$ is the variational approximation of the true predictive distribution $p(\mathbf{y}|\mathbf{z}_T)$. Likewise, we can calculate the empirical approximation of the term on the right hand side in Eq. (6) by following [1]:

$$\mathcal{L}_{\text{MI}} \approx \frac{1}{N} \sum_{n=1}^N \int p(\mathbf{z}_T|\mathbf{x}_T^n) \log q(\mathbf{y}^n|\mathbf{z}_T) d\mathbf{z}_T, \quad (7)$$

where n is the number of the X-ray image and EHR text pairs. In practice, \mathcal{L}_{MI} is implemented as a cross entropy loss.

3.4 Empirical Objective Function

By combining Eqs. (5) and (6), we obtain the following empirical objective function for optimization:

$$\begin{aligned} \tilde{\mathcal{L}}_{\text{VKD}} = & -\frac{1}{N} \sum_{n=1}^N \left[\frac{1}{M} \sum_{m=1}^M \log p(\mathbf{y}^n|\mathbf{x}_I, \mathbf{z}_I^{(m)}) - \frac{1}{L} \sum_{\ell=1}^L \log q(\mathbf{y}^n|\mathbf{z}_T^{(\ell)}) \right. \\ & \left. + D_{\text{KL}}[q(\mathbf{z}_T|\mathbf{x}_T^n)||p(\mathbf{z}_I|\mathbf{x}_I^n)] \right], \end{aligned} \quad (8)$$

where $\mathbf{z}_I^{(m)} \sim p(\mathbf{z}_I|\mathbf{x}_I)$, $\mathbf{z}_T^{(\ell)} \sim q(\mathbf{z}_T|\mathbf{x}_T)$, and L and M are the number of Monte Carlo samples. Note that we take the variational posterior $q(\mathbf{z}_T|\mathbf{x}_T)$ in Eq. (5) as the posterior $p(\mathbf{z}_T|\mathbf{x}_T)$ in Eq. (7). The resultant objective combines the strengths of the conditional variational auto-encoder and the variational information bottleneck, resulting in a new variational objective for knowledge distribution from EHR texts to X-rays for disease classification. Optimization with $\tilde{\mathcal{L}}_{\text{VKD}}$ is a process through which the model learns to read X-ray scans like a radiologist to find the relevant visual features to diseases.

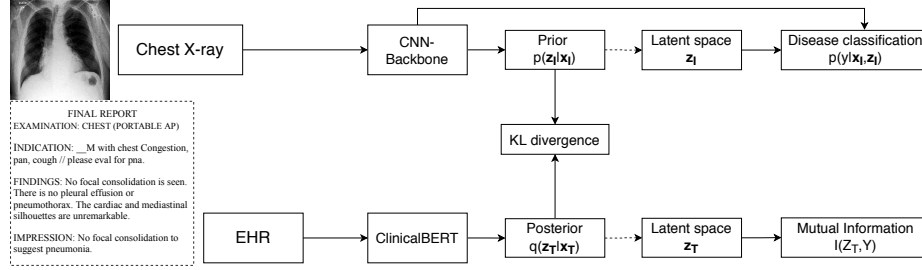


Fig. 1: Illustration of the proposed variational knowledge distillation from EHR texts to X-ray images.

3.5 Implementation with Neural Networks

We implement the optimization objective with deep neural networks (see Fig. 1) by adopting the amortization technique [15]. Both the variational posterior $q(\mathbf{z}_T|\mathbf{x}_T)$ and the prior $p(\mathbf{z}_I|\mathbf{x}_I)$ are parameterized as diagonal Gaussian distributions. To enable back propagation, we adopt the reparameterization trick [15] for sampling \mathbf{z} : $\mathbf{z}^{(\ell)} = f(\mathbf{x}, \epsilon^{(\ell)})$ with $\epsilon^{(\ell)} \sim \mathcal{N}(0, I)$, where $f(\cdot)$ is a deterministic differentiable function.

In prior $p(\mathbf{z}_I|\mathbf{x}_I)$, \mathbf{x}_I is taken as the representation of the X-ray image from a CNN. The inference network of the distribution parameters is implemented by a multi-layer perceptron (MLP). \mathbf{x}_T in the variational posterior $q(\mathbf{z}_T|\mathbf{x}_T)$ is generated through the use of deep contextualized word embeddings. The successful BERT [5] language model based on the Transformer [29] is used. More specifically, we use a pre-trained version of this model fine-tuned on a database with over two million EHRs [13]: ClinicalBERT [10]. To avoid computationally costly fine-tuning, the weights of ClinicalBERT are frozen and a brief fine-tuning step is applied by passing the embeddings through a single trainable Transformer encoder block ($\sim 1/12$ the size of ClinicalBERT). Similar to $p(\mathbf{z}_I|\mathbf{x}_I)$, the posterior $q(\mathbf{z}_T|\mathbf{x}_T)$ is also generated by an MLP.

Algorithm 1 demonstrates the learning process, when the model requires a multi-modal input: an image and the associated EHR. Once trained, the model performs disease classification based on new X-ray scans without the need of an EHR input at inference time, as can be seen in Algorithm 2.

Algorithm 1: Learning

Input: Training data: $(\mathbf{x}_I^n, \mathbf{x}_T^n, \mathbf{y}^n)$, $n = 1, \dots, N$,

Output: Latent space distributions $p(\mathbf{z}_I|\mathbf{x})$, $q(\mathbf{z}_T|\mathbf{x}_T)$,

- 1 **while** not converged: **do**
- 2 Draw Monte Carlo samples $\mathbf{z}_I^{(m)}$ and $\mathbf{z}_T^{(\ell)}$ from $p(\mathbf{z}_I|\mathbf{x}_I^n)$ and $q(\mathbf{z}_T|\mathbf{x}_T^n)$, respectively
- 3 Estimate the prediction distributions: $p(\mathbf{y}|\mathbf{x}_I^n, \mathbf{z}_I^{(m)})$ and $q(\mathbf{y}|\mathbf{z}_T^{(\ell)})$
- 4 Compute $\tilde{\mathcal{L}}_{VKD}$ in Eq. (8)
- 5 Update models weights via gradient descent on $\tilde{\mathcal{L}}_{VKD}$

Algorithm 2: Inference

Input: Testing data with only the X-Ray images \mathbf{x}_I^j .
Output: Prediction class label \mathbf{y}

- 1 Draw Monte Carlo samples $\mathbf{z}_I^{(\ell)}$ from the conditional prior $p(\mathbf{z}_I | \mathbf{x}_I^j)$
- 2 Estimate the prediction distribution $p(\mathbf{y} | \mathbf{x}_I^j, \mathbf{z}_I^{(\ell)})$

4 Experiments

4.1 Datasets

Three public chest X-ray datasets are used: 1) **MIMIC-CXR** [12] is the largest publicly available dataset containing full-text structured EHR and accompanying annotated chest X-rays [12]. The dataset contains 377,110 chest x-rays associated with 227,827 anonymized EHRs. Each EHR is associated with (multiple) frontal and/or sagittal X-ray views, each labelled according to specific classes (e.g. atelectasis, pneumothorax and pneumonia). 2) **OpenI** [20] is a similar public dataset with 7,470 chest X-rays associated with 3,955 anonymized EHRs. 3) **Chest X-ray14** [31] contains 112,120 chest X-rays, without associated EHRs. Paired EHRs exist for this dataset but they are not publicly available. Therefore, we use this dataset for testing but not for training.

Each image-EHR pair in these datasets is labelled according to a rule-based labelling procedure based on the EHR for fourteen distinct classes. MIMIC-CXR is labelled according to a different labeller [11] than Chest X-ray14 [31]. These different labelling procedures have an overlap in seven out of fourteen label classes. In this paper the classification labels in MIMIC-CXR are followed.

4.2 Experimental Settings

X-ray images are normalized and standardized to grayscale with dimensions of 224×224 , to align them with the DenseNet-121 CNN backbone, pre-trained on ImageNet [8]. Pre-trained CNN backbones have been proven effective in similar medical applications [21], and DenseNet-121 specifically has been proven ideal for X-ray images [22, 36]. Each EHR is tokenized according to WordPiece [34] tokenization, which has a library of around 30000 tokens. Each tokenized EHR is preceded by a [CLS] classification token and ended with a [SEP] token, following the methodology used in [5, 10]. The maximum number of tokens is set to 256. Shorter EHRs are zero padded to obtain text embeddings of the same sizes. The size of latent spaces \mathbf{z}_I and \mathbf{z}_T is set to an empirically determined value of 512. Two-layer MLPs with layer sizes $\{512, 512\}$ are used for the amortized inference of the prior and variational posterior. A dropout rate of 0.5 is applied to all layers, except the CNN backbone and the final layer in the generation of latent space \mathbf{z} , to which no dropout is applied. These architectures are trained on an NVIDIA RTX 2080ti GPU, using Adam [14] optimization for a duration defined by early stopping with a tolerance of 1%.

A common problem in optimizing variational architectures is KL vanishing. To prevent this, cyclical KL annealing [6] is applied according to Eq. 9, where the KL loss is multiplied with β_t . $g(\tau)$ is a monotonically increasing function, T is the number of batch iterations, t the current iteration, R (=0.5) determines the annealing grade and C (=4) is the number of annealing cycles per epoch:

$$\beta_t = \begin{cases} g(\tau), & \tau \leq R \\ 1, & \tau > R \end{cases}, \quad \text{where } \tau = \frac{\text{mod}(t - 1, [T/C])}{T/C} \quad (9)$$

4.3 Results

State-of-the-Art Comparison. The performance of our architecture in comparison with earlier works on image-based chest X-ray classification [19, 22, 31, 32, 36] is shown in Table 1. We report the results of the proposed method with and without variational knowledge distillation (i.e., no EHR). Results of our proposed method on the Chest X-ray14 dataset are obtained by fine-tuning a model pre-trained on MIMIC-CXR. Note that the fine-tuning step is necessary to alleviate domain shift between different datasets. Results on the OpenI and MIMIC-CXR datasets are obtained without any specific pre-training on radiology images from other datasets.

Results on the OpenI and MIMIC-CXR datasets show the performance gain due to knowledge distillation, where the performance improvement is consistent on the latter vastly larger dataset. It is worth mentioning that the high performance on Chest X-ray14 further indicates that the proposed variational knowledge distillation is transferable between datasets, even when the new tar-

| | Chest X-ray14 | | | | | OpenI | | | MIMIC-CXR | | |
|------------------|---------------|--------------|-------|-------|--------------|--------------|-------|------------------|--------------|------------------|--------------|
| | [22] | [36] | [31] | [3] | Ours | [31] | [19] | Ours (no EHR) | Ours | Ours (no EHR) | |
| No Finding | - | - | - | - | - | - | - | 0.711 | 0.720 | 0.825 | 0.827 |
| Enlarged | - | - | - | - | - | - | - | - | - | 0.589 | 0.838 |
| Cardiomeastinum | - | - | - | - | - | - | - | - | - | - | - |
| Cardiomegaly | 0.889 | 0.892 | 0.810 | 0.893 | 0.899 | 0.803 | - | 0.837 | 0.851 | 0.739 | 0.758 |
| Lung Opacity | - | - | - | - | - | - | - | 0.720 | 0.698 | 0.698 | 0.695 |
| Lung Lesion | - | - | - | - | - | - | - | 0.539 | 0.710 | 0.663 | 0.690 |
| Edema | 0.888 | 0.898 | 0.805 | 0.850 | 0.893 | 0.799 | - | 0.897 | 0.923 | 0.832 | 0.861 |
| Consolidation | 0.790 | 0.813 | 0.703 | 0.751 | 0.819 | 0.790 | - | 0.859 | 0.652 | 0.731 | 0.783 |
| Pneumonia | 0.768 | 0.767 | 0.658 | 0.739 | 0.781 | 0.642 | - | 0.610 | 0.619 | 0.618 | 0.627 |
| Atelectasis | 0.809 | 0.822 | 0.700 | 0.786 | 0.825 | 0.702 | - | 0.771 | 0.797 | 0.725 | 0.749 |
| Pneumothorax | 0.889 | 0.870 | 0.799 | 0.876 | 0.903 | 0.631 | - | 0.784 | 0.637 | 0.721 | 0.758 |
| Pleural Effusion | 0.864 | 0.881 | 0.759 | 0.832 | 0.871 | 0.890 | - | 0.904 | 0.858 | 0.864 | 0.892 |
| Pleural Other | - | - | - | - | - | - | - | 0.637 | 0.876 | 0.731 | 0.776 |
| Fracture | - | - | - | - | - | - | - | 0.486 | 0.532 | 0.557 | 0.698 |
| Support Devices | - | - | - | - | - | - | - | 0.553 | 0.581 | 0.854 | 0.897 |
| Average | - | 0.842 | 0.722 | 0.826 | 0.872 | 0.719 | 0.621 | 0.837 | 0.885 | 0.807 | 0.839 |

Table 1: Comparison of AUC values per class for NIH chest X-ray14 (partial), OpenI and MIMIC-CXR datasets.

| | OpenI | MIMIC-CXR |
|--------------------------------|--------------|--------------|
| Full architecture | 0.885 | 0.839 |
| w/o \mathcal{L}_{MI} (Eq. 7) | 0.873 | 0.832 |
| w/o VKD (no EHR) | 0.837 | 0.807 |

Table 2: AUC scores for varying architecture compositions.

| Size of \mathbf{z} | OpenI | MIMIC-CXR |
|----------------------|--------------|--------------|
| 64 | 0.814 | 0.775 |
| 128 | 0.870 | 0.829 |
| 512 - default | 0.885 | 0.839 |
| 1024 | 0.891 | 0.842 |

Table 3: AUC scores for varying size of latent space \mathbf{z} .

get dataset does not contain EHRs. Note that our approach outperforms all previous approaches for chest X-ray classification.

Ablation Studies. To verify the effectiveness of all elements in the proposed architecture two ablation studies are conducted. In the first ablation study, \mathcal{L}_{MI} (Eq. (7)) is left out of the objective function, thus there is no specific requirement for \mathbf{z}_T . Moreover, only the classification objective from the image branch is taken into account, removing the KL term, which results in a regular image-based classifier. This first ablation study (Table 2) reveals that the major contributing factor to the performance of our method shows to be variational knowledge distillation, whereas the addition of the objective function in the EHR branch (\mathcal{L}_{MI}) has a relatively smaller, yet considerable effect. Secondly, we test the effect of the size of latent space \mathbf{z} on the performance (Table 3). It appears that increasing the size of \mathbf{z} can improve model performance, while this effect tends to be smaller with larger values of \mathbf{z} . The current value of \mathbf{z} was chosen to be 512, which maximizes performance against computational cost.

Visualizations. The difference between \mathbf{z}_I with and without variational knowledge distillation is shown in Fig. 2. With variational knowledge distillation a structureness in classes within \mathbf{z}_I can be observed, whereas without it there

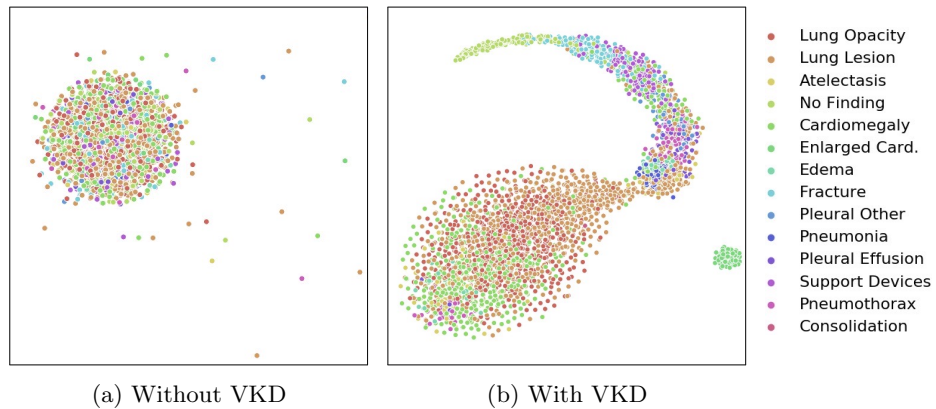


Fig. 2: t-SNE embeddings of latent space \mathbf{z}_I with and without VKD, overlaid with class labels, showing that VKD causes structuring of \mathbf{z}_I .

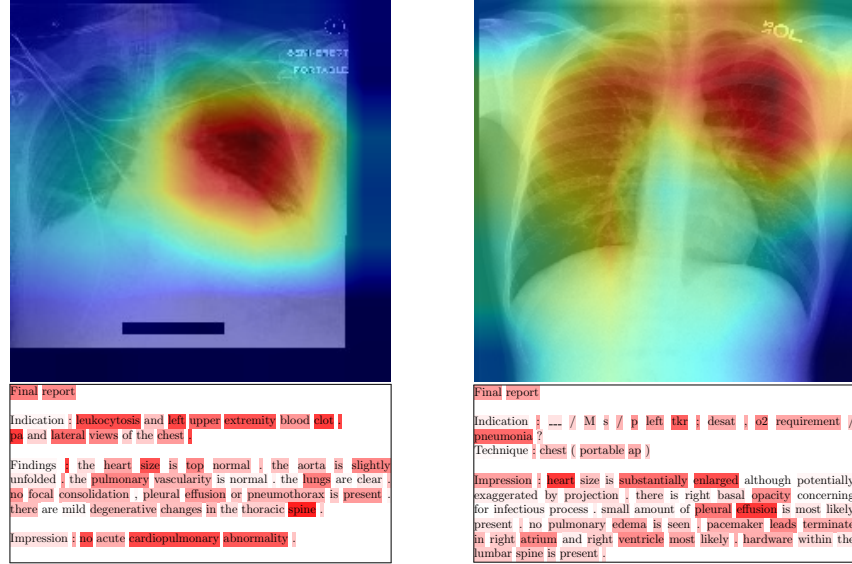


Fig. 3: Importance of words and image regions for two image-EHR pairs. Word-Piece tokens of the EHRs are averaged if needed to form full words. Darker red means higher importance.

seems to be more reliance on image tokens directly passed to the classification head, consequently resulting in a less structured z_1 . In Fig. 3 weight visualizations for the final CNN-layer with Grad-cam [24] and the final Transformer layer with BertViz [30] are shown for images and EHRs respectively. As can clearly be seen the visual focus is correctly on the lung region. Weights of the EHR tokens show a clear emphasis on important nouns and adjectives in the EHR. Verbs and prepositions show lower weights. These visualizations provide an intuitive illustration that our model is able to extract visual features relevant to the disease due to the proposed variational knowledge distillation.

5 Conclusion

In this paper, we propose a new probabilistic inference framework of multi-modal learning for disease classification based on X-rays by leveraging EHRs. We developed a latent variable model to learn latent representations of X-ray images. We introduce variational knowledge distillation that enables the model to acquire the ability to extract visual features relevant to the disease. This strategy enables us to incorporate the knowledge in EHRs during training, without relying on them in the testing stage. We conduct experiments on the current largest and most widely used chest X-ray - EHR datasets: MIMIC-CXR and OpenI, showing the benefit of variational knowledge distillation. Moreover we demonstrate our method performs well on Chest X-ray14 with only images by pre-training on MIMIC-CXR, which indicates its strong transfer ability across datasets.

References

1. Alemi, A.A., Fischer, I., Dillon, J.V., Murphy, K.: Deep variational information bottleneck. arXiv:1612.00410 (2016)
2. Cai, Q., Wang, H., Li, Z., Liu, X.: A Survey on Multimodal Data-Driven Smart Healthcare Systems: Approaches and Applications. *IEEE Access* **7**, 133583–133599 (sep 2019)
3. Chen, B., Li, J., Lu, G., Yu, H., Zhang, D.: Label co-occurrence learning with graph convolutional networks for multi-label chest x-ray image classification. *IEEE Journal of Biomedical and Health Informatics* (2020)
4. Chen, Y.C., Li, L., Yu, L., Kholy, A.E., Ahmed, F., Gan, Z., Cheng, Y., Liu, J.: Uniter: Learning universal image-text representations. arXiv:1909.11740 (2019)
5. Devlin, J., Chang, M.W., Lee, K., Toutanova, K.: Bert: Pre-training of deep bidirectional transformers for language understanding. arXiv:1810.04805 (2018)
6. Fu, H., Li, C., Liu, X., Gao, J., Celikyilmaz, A., Carin, L.: Cyclical annealing schedule: A simple approach to mitigating kl vanishing. arXiv:1903.10145 (2019)
7. Harerimana, G., Kim, J.W., Yoo, H., Jang, B.: Deep Learning for Electronic Health Records Analytics. *IEEE Access* **7**, 101245–101259 (2019)
8. He, K., Zhang, X., Ren, S., Sun, J.: Deep residual learning for image recognition. In: *IEEE CVPR* (June 2016)
9. Huang, G., Liu, Z., Van Der Maaten, L., Weinberger, K.Q.: Densely connected convolutional networks. In: *Proceedings of the IEEE CVPR*. pp. 4700–4708 (2017)
10. Huang, K., Altosaar, J., Ranganath, R.: Clinicalbert: Modeling clinical notes and predicting hospital readmission. arXiv:1904.05342 (2019)
11. Irvin, J., Rajpurkar, P., Ko, M., Yu, Y., Ciurea-Ilcus, S., Chute, C., Marklund, H., Haghgoo, B., Ball, R., Shpanskaya, K., et al.: Chexpert: A large chest radiograph dataset with uncertainty labels and expert comparison. In: *Proceedings of the AAAI Conference on Artificial Intelligence*. vol. 33, pp. 590–597 (2019)
12. Johnson, A.E., Pollard, T.J., Berkowitz, S., Greenbaum, N.R., Lungren, M.P., Deng, C.y., Mark, R.G., Horng, S.: Mimic-cxr: A large publicly available database of labeled chest radiographs. arXiv:1901.07042 (2019)
13. Johnson, A.E., Pollard, T.J., Shen, L., Li-wei, H.L., Feng, M., Ghassemi, M., Moody, B., Szolovits, P., Celi, L.A., Mark, R.G.: Mimic-iii, a freely accessible critical care database. *Scientific data* **3**, 160035 (2016)
14. Kingma, D.P., Ba, J.: Adam: A method for stochastic optimization. arXiv:1412.6980 (2014)
15. Kingma, D.P., Welling, M.: Auto-encoding variational bayes. In: *International conference on learning representations* (2014)
16. Li, Y., Wang, H., Luo, Y.: A comparison of pre-trained vision-and-language models for multimodal representation learning across medical images and reports. arXiv:2009.01523 (2020)
17. Liu, X., Faes, L., Kale, A.U., Wagner, S.K., Fu, D.J., Bruynseels, A., Mahendiran, T., Moraes, G., Shamdas, M., Kern, C., et al.: A comparison of deep learning performance against health-care professionals in detecting diseases from medical imaging: a systematic review and meta-analysis. *The lancet digital health* **1**(6), e271–e297 (2019)
18. Lu, J., Batra, D., Parikh, D., Lee, S.: Vilbert: Pretraining task-agnostic visiolinguistic representations for vision-and-language tasks. In: *Advances in Neural Information Processing Systems*. pp. 13–23 (2019)

19. Nunes, N., Martins, B., André da Silva, N., Leite, F., J. Silva, M.: A multi-modal deep learning method for classifying chest radiology exams. In: Lecture Notes in Computer Science. vol. 11804 LNAI, pp. 323–335. Springer Verlag (2019)
20. OpenI: Indiana university - chest x-rays (png images) openi.nlm.nih.gov/faq.php
21. Raghu, M., Zhang, C., Kleinberg, J., Bengio, S.: Transfusion: Understanding transfer learning for medical imaging. In: Advances in Neural Information Processing Systems. vol. 32. Curran Associates, Inc. (2019)
22. Rajpurkar, P., Irvin, J., Zhu, K., Yang, B., Mehta, H., Duan, T., Ding, D., Bagul, A., Langlotz, C., Shpanskaya, K., et al.: Chexnet: Radiologist-level pneumonia detection on chest x-rays with deep learning. arXiv:1711.05225 (2017)
23. Rezende, D.J., Mohamed, S., Wierstra, D.: Stochastic backpropagation and approximate inference in deep generative models. arXiv:1401.4082 (2014)
24. Selvaraju, R.R., Cogswell, M., Das, A., Vedantam, R., Parikh, D., Batra, D.: Grad-cam: Visual explanations from deep networks via gradient-based localization. In: Proceedings of the IEEE ICCV. pp. 618–626 (2017)
25. Sohn, K., Lee, H., Yan, X.: Learning structured output representation using deep conditional generative models. In: Advances in neural information processing systems. pp. 3483–3491 (2015)
26. Su, W., Zhu, X., Cao, Y., Li, B., Lu, L., Wei, F., Dai, J.: Vi-bert: Pre-training of generic visual-linguistic representations. arXiv:1908.08530 (2019)
27. Tan, H., Bansal, M.: Lxmert: Learning cross-modality encoder representations from transformers. arXiv:1908.07490 (2019)
28. Tobore, I., Li, J., Yuhang, L., Al-Handarish, Y., Kandwal, A., Nie, Z., Wang, L.: Deep learning intervention for health care challenges: Some biomedical domain considerations (2019)
29. Vaswani, A., Shazeer, N., Parmar, N., Uszkoreit, J., Jones, L., Gomez, A.N., Kaiser, L., Polosukhin, I.: Attention is all you need. In: Advances in neural information processing systems. pp. 5998–6008 (2017)
30. Vig, J.: A multiscale visualization of attention in the transformer model. arXiv:1906.05714 (2019)
31. Wang, X., Peng, Y., Lu, L., Lu, Z., Bagheri, M., Summers, R.M.: Chestx-ray8: Hospital-scale chest x-ray database and benchmarks on weakly-supervised classification and localization of common thorax diseases. In: Proceedings of the IEEE CVPR. pp. 2097–2106 (2017)
32. Wang, X., Peng, Y., Lu, L., Lu, Z., Summers, R.M.: Tienet: Text-image embedding network for common thorax disease classification and reporting in chest x-rays. In: Proceedings of the IEEE CVPR. pp. 9049–9058 (2018)
33. Weiskopf, N.G., Hripcsak, G., Swaminathan, S., Weng, C.: Defining and measuring completeness of electronic health records for secondary use. Journal of Biomedical Informatics **46**(5), 830 – 836 (2013)
34. Wu, Y., Schuster, M., Chen, Z., Le, Q.V., Norouzi, M., Macherey, W., Krikun, M., Cao, Y., Gao, Q., Macherey, K., et al.: Google’s neural machine translation system: Bridging the gap between human and machine translation. arXiv:1609.08144 (2016)
35. Xiao, C., Choi, E., Sun, J.: Opportunities and challenges in developing deep learning models using electronic health records data: a systematic review. Journal of the American Medical Informatics Association **25**(10), 1419–1428 (oct 2018)
36. Xue, Y., Huang, X.: Improved disease classification in chest x-rays with transferred features from report generation. In: International Conference on Information Processing in Medical Imaging. pp. 125–138. Springer (2019)